

First-Principles Study on the Crystalline Ga₄Sb₆Te₃ Phase Change Compound

Dario Baratella, Daniele Dragoni, Davide Ceresoli, and Marco Bernasconi*

The Ga₄Sb₆Te₃ compound on the GaSb–Sb₂Te₃ pseudobinary tie-line is proposed in the literature as a phase change material with high crystallization temperature. Herein, the crystal structure of this compound is uncovered by means of a genetic algorithm and electronic structure calculations based on density functional theory. As opposed to the parent GaSb compound which crystallizes in the zincblende structure, the Ga₄Sb₆Te₃ compound features an octahedral-like coordination for Ga as well as for Sb and Te atoms. Other structures close in energy to the ground state are also proposed, including some with a tetrahedral-like coordination of Ga atoms. Raman spectra computed within density functional perturbation theory and an empirical Bond Polarizability Model are shown to be able to discriminate among the different possible local environments of Ga atoms.

Phase change materials feature a fast and reversible transformation between the crystalline and amorphous phases induced by Joule heating that is exploited in the most mature emerging technology for new nonvolatile memories.^[1,2] The two phases of these materials display a large difference in the electrical conductivity that allows encoding the information, the read-out of the memory consisting of the measurement of the resistance at low bias. Stronger current pulses at higher bias are used in the programming operations by inducing the melting of the crystal and its subsequent amorphization (reset) or the recrystallization of the amorphous phase (set).^[3]

Phase change memories (PCMs) based on these principles entered the market in 2012 initially aiming at replacing NOR Flash memories.^[4] Further scaling of the devices led to the commercialization by Intel and Micron in 2017 of memories based

on the 3D Xpoint cross-bar technology^[5] that represent the first realization of the so-called storage-class memories, which would fill the performance gap between the fast but volatile DRAM and the nonvolatile but slow memories based on the Flash technologies.^[5,6] The flagship Ge₂Sb₂Te₅ phase change compound is used in these applications.^[1] The partial crystallization of Ge₂Sb₂Te₅ in an accumulation mode has also been exploited to mimic the operation of synapses in neuromorphic computing with PCMs.^[7,8]

PCMs are also emerging as a promising technology for embedded nonvolatile memories^[9] of interest in particular for automotive applications. These latter devices must operate at higher temperatures


than conventional stand-alone PCMs, and thus require crystallization temperatures higher than that of Ge₂Sb₂Te₅ which is reported in the range 150–170 °C.^[10] To this end, Ge-rich GeSbTe alloys have been selected with T_x higher than 300 °C resulting from phase separation into crystalline Ge and a less Ge-rich GeSbTe alloy.^[11] Other phase change materials with high T_x are also under scrutiny. Among these, the stoichiometric Ga₄Sb₆Te₃ compound has been shown to display a T_x of 271 °C, a high crystallization speed and good electrical contrast between the amorphous and crystalline phases.^[12] This composition is the only thermodynamically stable ternary compound reported so far in the Ga–Sb–Te phase diagram; as such it should be preferable to off-stoichiometric alloys which are prone to phase segregation that usually limits the endurance of the memory devices. Nevertheless, good performances for PCMs have been reported for the off-stoichiometric Ga₂Sb₅Te₃ composition as well.^[13]

The crystal structure of the stoichiometric Ga₄Sb₆Te₃ compound has been assigned to the rhombohedral crystalline system, but contrasting results have been obtained from X-ray diffraction (XRD) yielding a unit cell with lattice parameters $a = 4.28 \text{ \AA}$ and $c = 17.04 \text{ \AA}$ ^[12] or $a = 4.273 \text{ \AA}$ and $c = 11.306 \text{ \AA}$ ^[14] in the hexagonal notation. No other structural information is available, but the lattice parameters and the crystalline system. A detailed knowledge of the crystalline phase of Ga₄Sb₆Te₃ is, however, mandatory to understand the set/reset processes in the device at the atomistic level.

The Ga₄Sb₆Te₃ compound belongs to the pseudobinary tie-line GaSb–Sb₂Te₃. Its crystal structure is particularly intriguing because GaSb has a zincblend structure with Ga and Sb atoms in tetrahedral coordination, while Sb₂Te₃ crystallizes in a trigonal structure with atoms in a distorted octahedral coordination.^[15]

D. Baratella, Dr. D. Dragoni, Prof. M. Bernasconi
Dipartimento di Scienza dei Materiali
Università di Milano-Bicocca
Via R. Cozzi 55, I-20125 Milano, Italy
E-mail: marco.bernasconi@unimib.it

Dr. D. Ceresoli
Consiglio Nazionale delle Ricerche
Istituto di Scienze e Tecnologie Chimiche (CNR-SCITEC)
Via Golgi 19, I-20133 Milano, Italy

 The ORCID identification number(s) for the author(s) of this article can be found under <https://doi.org/10.1002/pssr.202000382>.

© 2020 The Authors. Published by Wiley-VCH GmbH. This is an open access article under the terms of the Creative Commons Attribution License, which permits use, distribution and reproduction in any medium, provided the original work is properly cited.

DOI: 10.1002/pssr.202000382

The Ga–Te binary compounds at the three known compositions, GaTe, Ga₂Te₃, and Ga₂Te₅, also crystallize in a tetrahedral-like geometry for Ga atoms.^[16–18] On the contrary, simulations based on density functional theory (DFT) showed that the tetrahedral coordination of Ga atoms and the octahedral/pyramidal coordinations of Sb and Te atoms present in the crystalline binary parent compounds survive in the amorphous phase of the ternary compound.^[19] It is therefore of interest to uncover which local configuration would be present in crystalline Ga₄Sb₆Te₃.

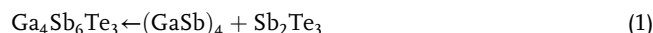
In this work, we attempted to identify the crystal structure of the Ga₄Sb₆Te₃ compound and its stability with respect to phase separation into the binary parent compounds by means of DFT atomistic simulations. To this end, we made use of a genetic algorithm implemented in the code USPEX^[20–22] that allows searching possible stable structures from the comparison of their DFT total energy computed with the code Siesta.^[23] The distribution of the energy of the different structures generated by USPEX in one simulation is reported in Figure S1, Supporting Information. There is a large group of structures at low energy, but among these only a few have an energy significantly lower than the others. The two structures with lowest energy found by USPEX were chosen for a further study with the Quantum-Espresso (QE) code.^[24]

The lowest energy structure of Ga₄Sb₆Te₃ found by the genetic algorithm belongs to the space group R-3m. This structure, named structure A, contains 13 atoms in the unit cell as shown in Figure 1a. It can also be described by the conventional hexagonal cell with 39 atoms and an ABC stacking of the atomic planes with one atom per plane along the *c*-axis. The structure consists of a main Ga₄Te₃ unit capped by a Sb₂ bilayer on both sides. A third Sb₂ bilayer is interposed between adjacent Sb₂–Ga₄Te₃–Sb₂ blocks. The lattice parameters in the hexagonal setting (three formula units, space group R-3m) are *a* = 4.152 Å and *c* = 67.65 Å. The atomic positions are given in Table S1,

Supporting Information. The *c*-axis is much longer than the experimental value of 17.04 Å reported in ref. [12]. However, we can conceive a degree of disorder in the size and distribution of the interposed Sb₂ bilayers, as occurs, for instance, in the (GeTe)_{*n*}–Sb₂Te₃ crystals grown by molecular beam epitaxy, which display a disorder in the size of the GST blocks as revealed by transmission electron microscopy (TEM).^[25] We could therefore conceive that the *c*-axis measured experimentally by XRD might actually be the average thickness of the blocks. The thickness of the Sb₂–Ga₄Te₃–Sb₂ block, for instance, is 16.66 Å which is not too far from the experimental value.

The second structure with lowest energy found by USPEX, that we named structure B, is very similar to structure A, just differing by a permutation of the outer Sb₂ bilayer with one external GaTe bilayer (see Figure 1b). The cell parameters (three formula units, space group R3m) of *a* = 4.14 Å and *c* = 68.57 Å are very similar to those of structure A. The atomic positions are given in Table S2, Supporting Information.

We calculated the formation energy at zero temperature from the reaction



which is defined by $\Delta H = E(\text{Ga}_4\text{Sb}_6\text{Te}_3) - 4E(\text{GaSb}) - E(\text{Sb}_2\text{Te}_3)$. We obtain $\Delta H = -23.2 \text{ meV atom}^{-1}$ and $\Delta H = -19.5 \text{ meV atom}^{-1}$ for structures A and B. On this basis, both structures A and B are stable with respect to phase separation in the parent binary compounds. The total energies of the ternary and parent compounds are computed with the QE code. Both structures A and B are metallic as shown by the electronic density of states in Figure 2. The band structure of the most stable structure A is shown in Figure S2, Supporting Information. The electronic density of states (DOS) projected on different

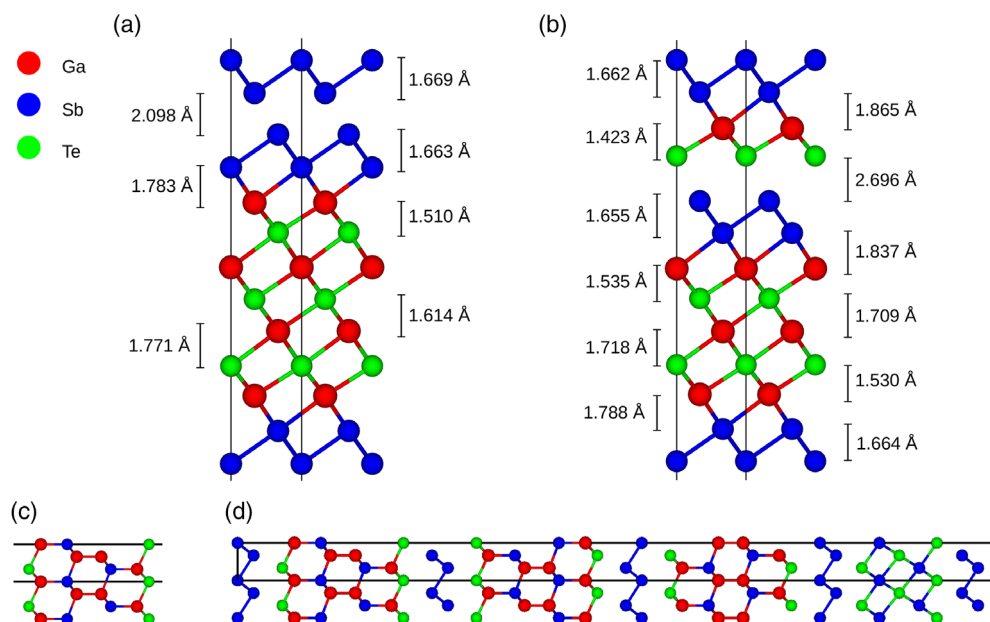


Figure 1. a) Structure A and b) structure B of Ga₄Sb₆Te₃. The unit cell contains 13 planes with a single atom per plane for both structures. c) Structure of the Ga₄Sb₂Te₂ unit and d) structure C of Ga₄Sb₆Te₃. The unit cell in panel (d) contains 39 planes with one atom per plane. The atomic positions in crystal coordinates of structures A, B, and C are given in the Supporting Information.

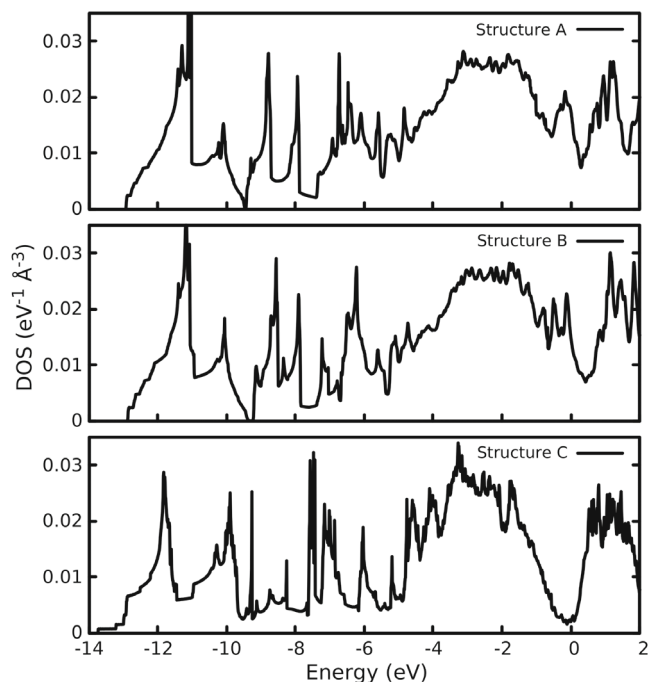


Figure 2. Electronic DOS of $\text{Ga}_4\text{Sb}_6\text{Te}_3$ in structures A, B, and C. The DOS is aligned at the Fermi level at zero energy. The DOS is computed with the tetrahedron method on a $24 \times 24 \times 24$ mesh in the Brillouin Zone. The DOS at the Fermi level is 0.017, 0.0142, and 0.0019 states $\text{eV}^{-1}\text{Å}^{-3}$ for structures A, B, and C, respectively.

atomic species for structures A is shown in Figure S3, Supporting Information.

In the low energy structures found by USPEX, all atoms are in an octahedral coordination. In the search that led to this result we gave as possible starting point in the genetic algorithm some structures with mixed octahedral and tetrahedral coordination. Some of these structures are described in the following, although they are higher in energy than structures A and B described earlier. The first of the tetrahedral-like structures is based on a $\text{Ga}_4\text{Sb}_2\text{Te}_2$ unit. This unit is similar to the main unit present in the GaTe crystal. It has a hexagonal structure with eight hexagonal planes, but here the stacking is ABBCAAB. The Te atoms occupy the two external planes, while a gallium dimer is present at the center of the slab. Ga and Sb atoms have a tetrahedral coordination and they are stacked along c as in the [111] direction of the ZnS crystal. The geometry of this unit is shown in Figure 1c. We then envisaged the possibility to stack the $\text{Ga}_4\text{Sb}_2\text{Te}_2$ units along with Sb_2Te_3 and Sb_2 blocks to build ternary alloys with different compositions. On this basis, we built a model of the $\text{Ga}_4\text{Sb}_6\text{Te}_3$ compound as $3(\text{Ga}_4\text{Sb}_6\text{Te}_3) = 3(\text{Ga}_4\text{Sb}_2\text{Te}_2) + 5(\text{Sb}_2) + (\text{Sb}_2\text{Te}_3)$ in a hexagonal cell with 39 atoms. The optimized model, named structure C with space group P3m1, is shown in Figure 1d. The equilibrium lattice parameters in the hexagonal setting (three formula units) are $a = 4.222 \text{ Å}$ and $c = 74.54 \text{ Å}$. The atomic positions of structure C are shown in Table S3, Supporting Information.

The formation energy with respect to the parent compounds (see Equation (1)) at zero temperature is about -1 meV atom^{-1} which means that structure C is only marginally stable with

respect to phase separation. As opposed to phases A and B, phase C has a pseudogap at the Fermi level (see Figure 2).

We built still another structure of $\text{Ga}_4\text{Sb}_6\text{Te}_3$ with Ga in tetrahedral coordination but with no Ga–Ga dimers. This structure was built from the $(\text{GaSb})_3/\text{Sb}_2$ block that was proposed in ref. [26] where $(\text{GaSb})_n/\text{Sb}$ superlattices were discussed. This unit is made of a $(\text{GaSb})_3$ block in a ZnS geometry capped by a Sb_2 bilayer on one side to have a Sb outermost layer on both sides. The structure of the block is shown in the center of Figure S4a, Supporting Information. We then built a superlattice made of a $(\text{GaSb})_3/\text{Sb}_2$ unit and a Sb_2Te_3 unit which leads to the superlattice $\text{Ga}_3\text{Sb}_5/\text{Sb}_2\text{Te}_3$ (space group R3m) shown in Figure S4a, Supporting Information. The superlattice is at a slightly different composition than $\text{Ga}_4\text{Sb}_6\text{Te}_3$. To recover the alloy at the right composition, we built a $2 \times 1 \times 1$ supercell with 26 atoms. We substituted one of the Sb atoms in the planes of the Sb_2Te_3 block with a Ga atom. In this way, the Sb_2Te_3 unit becomes a SbGaTe_3 block and the composition $\text{Ga}_4\text{Sb}_6\text{Te}_3$ is recovered. The optimized cell, named structure D, is shown in Figure S4b, Supporting Information. The equilibrium lattice parameters (three formula units, no symmetry because of the Ga/Sb substitution in the SbGaTe_2 block) are $a = 4.261 \text{ Å}$ and $c = 70.137 \text{ Å}$. The atomic positions of structure D and of the $\text{Ga}_3\text{Sb}_5/\text{Sb}_2\text{Te}_3$ superlattice are shown in Table S4 and S5, Supporting Information. The formation energy (Equation (1)) of structure D is $\Delta H = 45.2 \text{ meV atom}^{-1}$; it is actually positive which means that this structure is unstable with respect to phase separation into the parent compounds. A similar value of $50.8 \text{ eV atom}^{-1}$ is obtained for the composition $\text{Ga}_3\text{Sb}_7\text{Te}_3$ in the $\text{Ga}_3\text{Sb}_5/\text{Sb}_2\text{Te}_3$ superlattice configuration. Structure D is also metallic, while the structure with composition $\text{Ga}_3\text{Sb}_7\text{Te}_3$ is semiconducting (see Figure S7, Supporting Information). The electronic DOS projected on different atomic species for structures B–D is shown in Figure S3, Supporting Information. Although the electronic DOS is different in the different structures, the discrimination of the structure on the basis of its electronic conductivity might be impractical. As a matter of fact, we expect the Fermi level to shift considerably in the real system due to defects in stoichiometry with respect to the ideal structures considered here as occurs, for instance, in GeSbTe alloys.^[27,28] On the contrary, the different local atomic coordination in structures A–D is expected to give rise to different vibrational spectra which could be detected by Raman spectroscopy. To address this issue, we have computed phonons at the Γ -point for the competitive structures A–C by density functional perturbation theory (DFPT)^[29] as implemented in the QE code. As some crystals are metallic, the Raman tensor cannot be computed from first principles in nonresonant conditions as we did previously for $\text{Ge}_2\text{Sb}_2\text{Te}_5$.^[30] Here, we used instead a Bond Polarizability Model (BPM)^[31,32] that we also developed for GeSbTe alloys in ref. [33]. For GaSbTe we used a simplified BPM with just a single set of parameters equal for all types of bonds corresponding to those of the Sb–Te (long) bond for GeSbTe fitted in our previous work (see Table I of ref. [33] and the discussion thereby for details). The resulting Raman spectra are thus not expected to provide reliable Raman intensities, but they can be used anyway to highlight the main spectroscopic features and their dependence on the crystal structure.

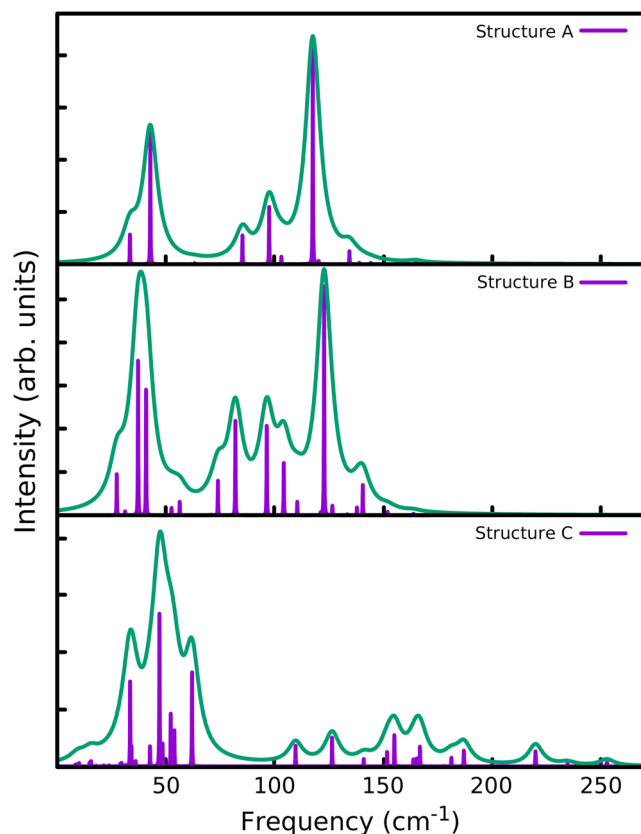


Figure 3. Raman spectra from ab initio phonons and a simplified BPM for structures A–C of $\text{Ga}_4\text{Sb}_6\text{Te}_3$. The spectra are computed for nonpolarized light in backscattering geometry for a polycrystalline sample. The phonon frequencies are smeared with Lorentzian functions either 4 or 0.1 cm^{-1} wide. Raman peaks of structure C above 150 cm^{-1} are due to vibrations of the single Sb bilayer and to stretching modes of tetrahedral Ga–Te, Ga–Sb and Ga–Ga bonds as described in the text.

The Raman spectra for nonpolarized light in backscattering geometry for a polycrystalline sample are shown in **Figure 3** for structures A–C of $\text{Ga}_4\text{Sb}_6\text{Te}_3$. The frequency and character of the most Raman active Γ -point phonons for structures A and B are shown in **Table 1**. The full set of Γ -point phonons for structures A and B are shown in Tables S6 and S7, Supporting Information. The displacement pattern of the most Raman active modes in structures A, B, and C is shown in Figure S6–S9, Supporting Information.

While in structures A and B there are no modes above 166 cm^{-1} , the Raman spectrum of structure C displays peaks above 250 cm^{-1} which are due to stretching modes of the Ga–Ga dimer and peaks in the range $200\text{--}230\text{ cm}^{-1}$ due to stretching modes of the Ga–Sb bonds with Ga in tetrahedral configurations. Indeed, the Raman spectrum of bulk GaSb shows two peaks at 226 and 220 cm^{-1} due to longitudinal optical and transverse optical modes.^[34] The bending of the Ga–Ga dimer is at about 220 cm^{-1} as well. Raman peaks at 155 and 187 cm^{-1} are due to E and A modes of the single Sb bilayer which are very close to the two modes of a self-standing bilayer.^[35] The E and A

Table 1. Frequency and character of the most Raman active Γ -point phonons of $\text{Ga}_4\text{Sb}_6\text{Te}_3$ in structures A and B.

Structure A		Structure B	
Mode	Frequency [cm^{-1}]	Mode	Frequency [cm^{-1}]
$E_g(1)$	33	$E(3)$	31
$A_{1g}(1)$	43	$A_1(2)$	37
$E_g(2)$	63	$A_1(3)$	41
$A_{1g}(2)$	85	$E(4)$	53
$E_g(3)$	97	$E(5)$	56
$E_g(4)$	103	$E(6)$	71
$A_{1g}(3)$	118	$A_1(4)$	74
$E_g(5)$	120	$A_1(5)$	82
$A_{1g}(4)$	134	$A_1(6)$	96
$E_g(6)$	139	$E(8)$	104
$A_{1g}(5)$	144	$A_1(8)$	123
$A_{1g}(6)$	165	$A_1(10)$	141

modes of vibration of the Sb bilayer in structure A are instead at lower frequencies due to couplings with the Sb capping layers of the Ga–Te block (see Figure S6, Supporting Information). The peak at 167 cm^{-1} in structure C is due to vibrations of tetrahedral Ga–Te bonds. The intense peaks at 62 and 110 cm^{-1} are due instead to vibrations inside the Sb_2Te_3 block which are close in frequency to those of bulk Sb_2Te_3 .^[36]

In conclusion, DFT calculations have provided some models for the crystal structure of $\text{Ga}_4\text{Sb}_6\text{Te}_3$. In the structure with the lowest energy (structure A), actually found by means of a genetic algorithm, all atoms are octahedrally coordinated, in part, with the trigonal distortion typical of crystalline Sb. However, another structure with Ga atoms and part of Sb atoms in a tetrahedral coordination (structure C) is competitive in energy within few tens of meV atom^{-1} . As structures A and C also have similar in-plane lattice parameters, they might lead to a coexistence of octahedral and tetrahedral geometries in the real samples. We further remark that simulations with USPEX with variable compositions also yielded a $(\text{GaSb})_2\text{--Sb}_2\text{Te}_3$ pseudobinary compound in a layered structure with octahedral-like atomic coordination similar to that of structure A of $\text{Ga}_4\text{Sb}_6\text{Te}_3$ (see Figure S10 and Table S9, Supporting Information). This $\text{Ga}_2\text{Sb}_4\text{Te}_3$ compound is stable with respect to the decomposition in the parent binary compounds with a reaction energy of -21 meV atom^{-1} . We can thus envisage the possibility of a disorder in the size and composition of GaSbTe blocks as occurs for GeSbTe alloys.^[25] To make a contact with future experimental studies on this system, we computed the Raman spectra of these structures by using DFT phonons and the BPM. We found that the Ga–Ga dimers and Ga–Sb and Ga–Te bonds in a tetrahedral geometry give rise to different vibrational features that would allow discriminating among the different possible structures from the analysis of the Raman spectra. Experimental Raman spectra are not available at the moment, and we hope that our findings could stimulate future experimental work in this direction.

Computational Details

The USPEX code exploits a genetic algorithm to generate several possible structures with a fixed or variable number of atoms per unit cell.^[20–22] The selection of the structure in each generation is made on the basis of the total energy computed within DFT with the Siesta code^[23] which uses an atomic-like basis set for the expansion of Kohn–Sham orbitals. We used norm conserving pseudopotential and the Perdew–Burke–Ernzerhof^[37] approximation to the exchange and correlation functional. Each structure was locally optimized in three different steps. In the first step, atomic positions only were relaxed while cell vectors were kept fixed. The threshold on forces was 0.5 eV \AA^{-1} and the wave function was expanded in a minimal basis set. In the second step, cell vectors were relaxed as well; the basis set was increased to a double- ζ and the thresholds on forces and stress were decreased to 0.25 eV \AA^{-1} and 1 GPa . Finally, in the last step the basis set was increased to a double- ζ with polarization, while the threshold on forces was set to 0.1 eV \AA^{-1} . The spacing Δk for Brillouin Zone integration was 0.10 , 0.08 , and 0.06 \AA^{-1} for the first, second, and last step of relaxation.

The structures generated randomly by USPEX were taken from the 143 to the 194 space groups because experimentally this alloy was assigned to a trigonal or hexagonal space group. In total, three different USPEX simulations were made at fixed compositions. In the first, a fixed number of 13 atoms per cell was used. The calculation found a group of structures at the lowest energy minima after 38 generations, each one with 30 different structures. In the other two simulations, with a fixed number of 26 or 39 atoms per cell, no structures with energy lower than those obtained with the smallest cell were found. A fourth simulation was made with variable composition with the constraint to lie on the GaSb–Sb₂Te₃ pseudobinary line.

The two structures with lowest energy found by USPEX were chosen for a further study with the QE code^[24] which exploits a plane waves expansion of Kohn–Sham orbitals, and it provides a more accurate calculation of the total energy than that possible within the setting used for the USPEX simulations. A $12 \times 12 \times 12$ or $8 \times 8 \times 8$ Monkhorst–Pack^[38] meshes were used for Brillouin Zone integration. Optimization of the cell was performed with a high energy cutoff of 80 Ry in the expansion of Kohn–Sham orbital to minimize the Pulay stress in the search of the equilibrium (zero stress) configuration with a quasi-Newton method implemented in the QE code. The correction due to Grimme^[39] was added to include van der Waals interactions in a semiempirical manner.

Supporting Information

Supporting Information is available from the Wiley Online Library or from the author.

Acknowledgements

This project has received funding from the European Union's Horizon 2020 research and innovation programme under grant agreement no. 824957.

Conflict of Interest

The authors declare no conflict of interest.

Keywords

density functional theory, electronic structure calculations, phase change memories

Received: August 9, 2020

Revised: September 3, 2020

Published online: September 22, 2020

- [1] M. Wuttig, N. Yamada, *Nat. Mater.* **2007**, *6*, 824.
- [2] W. Zhang, R. Mazzarello, M. Wuttig, E. Ma, *Nat. Rev. Mater.* **2019**, *4*, 150.
- [3] P. Noé, C. Vallée, F. Hippert, F. Fillot, J.-Y. Raty, *Semicond. Sci. Technol.* **2018**, *33*, 013002.
- [4] P. Fantini, *J. Phys. D: Appl. Phys.* **2020**, *53*, 283002.
- [5] J. Choe, <http://www.techinsights.com/about-techinsights/overview/blog/intel-3d-xpoint-memory-die-removed-from-intel-optane-pcm> (accessed: September 2020).
- [6] S. W. Fong, C. M. Neumann, H.-S. P. Wong, *IEEE Trans. Electron Devices* **2017**, *64*, 4374.
- [7] D. Kuzum, R. G. Jayasingh, B. Lee, H. S. Wong, *Nano Lett.* **2012**, *12*, 2179.
- [8] I. Boybat, M. Le Gallo, S. R. Nandakumar, T. Moraitis, T. Parnell, T. Tuma, B. Rajendran, Y. Leblebici, A. Sebastian, E. Eleftheriou, *Nat. Commun.* **2018**, *9*, 2514.
- [9] P. Cappelletti, R. Annunziata, F. Arnaud, A. Disegni, F. Maurelli, P. Zuliani, *J. Phys. D: Appl. Phys.* **2020**, *53*, 193002.
- [10] P. Noé, C. Sabbione, N. Bernier, N. Castellani, F. Fillot, F. Hipper, *Acta Mater.* **2016**, *110*, 142.
- [11] P. Zuliani, E. Palumbo, M. Borghi, G. Dalla Libera, R. Annunziata, *Solid-State Electron.* **2015**, *111*, 27.
- [12] H. Cheng, S. Raoux, J. Jordan-Sweet, *Appl. Phys. Lett.* **2011**, *98*, 121911.
- [13] K.-F. Kao, C.-M. Lee, M.-J. Chen, M.-J. Tsai, T.-S. Chin, *Adv. Mater.* **2009**, *21*, 1695.
- [14] C.-M. Lee, W.-S. Yen, J.-P. Chen, T.-S. Chin, *IEEE Trans. Magn.* **2005**, *41*, 1022.
- [15] T. Anderson, H. Krause, *Acta Crystallogr. B* **1974**, *30*, 1307.
- [16] M. Julien-Pouzol, S. Jaulmes, M. Guittard, F. Alapini, *Acta Crystallogr. B* **1979**, *35*, 2848.
- [17] A. Kolobov, P. Fons, M. Krbal, K. Mitrofanov, J. Tominaga, T. Uruga, *Phys. Rev. B* **2017**, *95* 054114.
- [18] H. Deiseroth, P. Amann, *Angew. Chem.* **1996**, *622*, 985.
- [19] A. Bouzid, S. Gabardi, C. Massobrio, M. Boero, M. Bernasconi, *Phys. Rev. B* **2015**, *91*, 184201.
- [20] A. Oganov, C. Glass, *J. Chem. Phys.* **2006**, *124*, 244704.
- [21] A. Oganov, H. Stokes, M. Valle, *Acc. Chem. Res.* **2011**, *44*, 227.
- [22] A. O. Lyakhov, A. Oganov, H. Stokes, Q. Zhu, *Comput. Phys. Commun.* **2013**, *184*, 1172.
- [23] J. Soler, E. Artacho, J. D. Gale, A. García, J. Junquera, P. Ordejon, D. Sanchez-Portal, *J. Phys.: Condens. Matter* **2002**, *14*, 2745.
- [24] P. Giannozzi, O. Andreussi, T. Brumme, O. Bunau, M. Buongiorno Nardelli, M. Calandra, R. Car, C. Cavazzoni, D. Ceresoli, M. Cococcioni, N. Colonna, I. Carnimeo, A. Dal Corso, S. de Gironcoli, P. Delugas, R. A. DiStasio, A. Ferretti, A. Floris, G. Fratesi, G. Fugallo, R. Gebauer, U. Gerstmann, F. Giustino, T. Gorni, J. Jia, M. Kawamura, H.-Y. Ko, A. Kokalj, E. Küçükbenli, M. Lazzeri, et al., *J. Phys.: Condens. Matter* **2017**, *29*, 465901.
- [25] J. Momand, R. Wang, J. Boschker, M. Verheijen, R. Calarco, B. Kooi, *Nanoscale* **2017**, *9*, 8774.
- [26] Y. Lu, M. Wang, S. Song, M. Xia, Y. Jia, X. Shen, S. Wang, G. Dai, Z. Song, *Appl. Phys. Lett.* **2016**, *109*, 173103.
- [27] B.-S. Lee, J. R. Abelson, S. G. Bishop, D.-H. Kang, B.-K. Cheong, K.-B. Kim, *J. Appl. Phys.* **2005**, *97*, 093509.
- [28] S. Caravati, M. Bernasconi, T. Kühne, M. Krack, M. Parrinello, *J. Phys.: Condens. Matter* **2009**, *21*, 255501.
- [29] S. Baroni, S. de Gironcoli, A. Dal Corso, *Rev. Mod. Phys.* **2001**, *73*, 515.
- [30] G. Sosso, S. Caravati, C. Gatti, S. Assoni, M. Bernasconi, *J. Phys.: Condens. Matter* **2009**, *21*, 245401.
- [31] M. V. Volkenstein, *C. R. Acad. Sci. USSR* **1941**, *30*, 791.
- [32] M. Eliashevich, M. Volkenstein, *J. Phys.* **1944**, *9*, 101.

- [33] G. Sosso, S. Caravati, R. Mazzarello, M. Bernasconi, *Phys. Rev. B* **2011**, *83*, 134201.
- [34] Y. K. Su, K. J. Gan, J. S. Hwang, S. L. Tyan, *J. Appl. Phys.* **1990**, *68*, 5584.
- [35] D. Campi, M. Bernasconi, G. Benedek, *Phys. Rev. B* **2012**, *86*, 075446.
- [36] G. C. Sosso, S. Caravati, M. Bernasconi, *J. Phys.: Condens. Matter* **2009**, *21*, 095410.
- [37] J. P. Perdew, K. Burke, M. Ernzerhof, *Phys. Rev. Lett.* **1996**, *77*, 3865.
- [38] H. Monkhorst, J. D. Pack, *Phys. Rev. B* **1976**, *13*, 5188,.
- [39] S. Grimme, J. Antony, S. Ehrlich, H. Krieg, *J. Chem. Phys.* **2010**, *132*, 154104.